Available online at www.sciencedirect.com
SCIENCE DIRECT®
PERGAMON
International Journal of Rock Mechanics & Mining Sciences 40 (2003) 389–403
International Journal of Rock Mechanics and Mining Sciences
www.elsevier.com/locate/ijrmms

Effects of pressure and saturating fluid on wave velocity and attenuation in anisotropic rocks

J.M. Carcione[a,*], K. Helbig[b], H.B. Helle[c]

[a] *Istituto Nazionale di Oceanografia e di Geofisica Sperimentale-OGS, Borgo Grotta Gigante 42C, 34010 Sgonico, Trieste, Italy*
[b] *Kiebitzrain 84, D 30657 Hannover, Germany*
[c] *Norsk Hydro a.s., E & P Research Centre, N-5020 Bergen, Norway*

Accepted 24 January 2003

Abstract

We obtain the energy velocities and quality factors of anisotropic reservoir rocks as a function of pore pressure, partial saturation and frequency. The model is based on Biot's poroelastic theory for anisotropic media. The directional dependence of attenuation is obtained by generalizing the eigenstiffnesses of the undrained medium to relaxation functions (six at most, depending on the material symmetry). The frequency dependence of attenuation is described with constant-Q kernels associated with each eigenstiffness, and viscodynamic functions to model the high-frequency behavior. We apply a uniform gas/fluid mixing law that satisfies Reuss's and Voigt's averages at low and high frequencies, respectively, thus, simulating the unrelaxed state due to non-uniform—patchy—saturation (segregated fluids). Pressure effects are accounted for by an effective stress law.

1. Introduction

Seismic measurements of wave velocity and attenuation can be interpreted to give accurate estimations of pore pressure and fluid saturation. These measurements can be utilized for a wide range of applications, including rock mechanics, civil and mining engineering, and exploration geophysics. Oil production, for instance, changes the pore pressure and the stress state of the reservoir. This phenomenon is closely related to anisotropy in the transport properties. Fractures and cracks have a large influence on the permeability of reservoirs, since their orientations dictate the directions of preferential fluid flow. Seismic measurements of wave velocity and attenuation can be used for reservoir characterization (provided that the effects of pore-fluid pressure on those quantities are known). On the other hand, pore-fluid pressure affects the aperture of fracture and cracks. The effect of crack aperture on seismic anisotropy is well understood. Therefore, changes in seismic anisotropy can be used to determine changes in pore pressure. Knowledge of pore-fluid pressure is essential in planning the drilling process to control potentially dangerous abnormal pressures, and to characterize the reservoir properties.

In terms of seismic measurements, a reservoir containing a set of fractures (or cracks) can be described by a porous medium that is effectively anisotropic. An originally porous medium containing a set of cracks is transversely isotropic (with the axis perpendicular to the plane of the cracks). If the medium has additional structure (layering, grain orientation, etc.), higher anisotropy results (orthorhombic, monoclinic) [1]. Moreover, attenuation can be modeled by using the concept of eigenstrain [2,3], by which a medium can be described by at most six relaxation functions. The resulting rock-physics model is an anisotropic, viscoelastic porous medium.

Anisotropic poroelasticity was introduced by Biot [4,5] and Biot and Willis [6] in terms of bulk parameters of total stress and strain. To our knowledge, Brown and Korringa [7] were the first to obtain the material coefficients in terms of the properties of the grain, pore-fluid and frame. Later, Carroll [8] and Thompson and Willis [9] presented further micromechanical

*Corresponding author. Tel.: +39-040-2140345; fax: +39-040-327521.
E-mail addresses: jcarcione@ogs.trieste.it (J.M. Carcione), hans.b.helle@nho.hydro.com (H.B. Helle).

1365-1609/03/$ - see front matter
doi:10.1016/S1365-1609(03)00016-9

analysis of the constitutive equations. Recently, Cheng [10] related the Hookean constants to the engineering constants (obtained from laboratory measurements), including explicit relations for the orthorhombic and transverse isotropy material symmetries. This theory assumes that the solid constituent is isotropic and that anisotropy is due to arrangements of the grains (i.e., the frame is anisotropic). Complete experimental data for anisotropic media are scarce. Experiments on real rocks can be found in Lo et al. [11], Aoki et al. [12] and Rasolofosaon and Zinszner [13]. Wave propagation in anisotropic poroelastic rocks is investigated by Norris [14], Ben-Menahem and Gibson [15], Parra [16], and Gelinsky and Shapiro [17] and Gelinsky et al. [18], who study layered systems and the effects of anisotropic permeability. Carcione [19,20] investigates the wave properties in an anisotropic poroviscoelastic medium, obtaining the expressions of measurable quantities and fundamental relations between them.

Hudson [21] and Tod [22] use a micro-structural theory of cracked rock to study the effects of stress and fluid pressure on anisotropy. The pressure effects are included via a mechanism that allows for the closure of the cracks under applied stress, without considering hysteresis and damage effects. Moreover, the crack distribution is isotropic in the unstressed state.

We describe the frequency dependence of attenuation by using a constant-Q model for the wet-rock stiffness components [23,24]. This approach is phenomenological, since a theory describing all the possible attenuation mechanisms present in a real sandstone or limestone is difficult, if not impossible, to develop. The constant-Q kernel is the most simple model based on only one parameter. Keller [25] has used this kernel to model frame anelasticity in Biot's theory for isotropic saturated media. He obtained good fits of experimental P-wave attenuation and velocity of sediments. Here, we assume that low stiffness is accompanied by a low quality factor (high attenuation). Moreover, we introduce high-frequency viscodynamic effects, based on an optimal viscodynamic function proposed by Johnson et al. [26].

Various physical processes cause anomalous pressures in an underground fluid. The two most common causes are cracking, i.e., oil-to-gas conversion [27], and non-equilibrium or disequilibrium compaction [28]. Oil-to-gas cracking may cause the pore pressure to reach or exceed the lithostatic pressure [29]. One speaks of disequilibrium compaction if deposition occurs so fast that the fluids cannot be expelled from the shrinking pore space. In this situation, the fluids carry part of the load that would be held by grain contacts, and abnormal pore pressures develop in the pore space. A description of this mechanism is given by Rubey and Hubbert [30].

Pressure effects are introduced by using an effective stress law. At constant effective pressure the acoustic (or transport) properties of the rock remain constant. The effective pressure depends on the difference between the confining and pore pressures, the latter multiplied by the effective stress coefficient. In general, this coefficient is not equal to unity and therefore, Terzaghi's effective pressure law (that is, the effective pressure is the differential pressure) is not appropriate to describe the acoustic properties of the rock versus varying pore pressure. However, a proper determination of the effective stress coefficients requires measurements of wave velocity as a function of confining and pore pressure. To our knowledge, a complete data set has not been published for anisotropic rocks. As Zimmerman shows [31], the dry-rock effective stress coefficient is equal to 1, provided the rock is composed of a linear elastic grain material and the properties do not depend on the length scale of the pore structure; at least this is rigorously true for isotropic materials.

The effect of partial saturation on velocity and attenuation depends on the frequency range. At low frequencies, the fluid has enough time to achieve pressure equilibration (relaxed regime). In this case, Reuss's model for the bulk modulus of the fluid mixture yields results that agree with the experiments. At high frequencies the fluid cannot relax and this state of unrelaxation induces a stiffening of the pore material, which increases the wave velocity considerably [32]. This effect implies an uneven distribution of fluids in the pore space, which is normally called patchy saturation. In this case Reuss's model is not appropriate and, in general, Hill's average is used to model the wave velocities at ultrasonic (laboratory) frequencies [33]. No microstructural theory is able to predict the behavior at intermediate frequencies. In the present model, we use a modified empirical fluid mixing law proposed by Brie et al. [34], which gives Reuss's modulus at low frequencies and Voigt's modulus at high frequencies.

In the following, the spatial variables x, y and z are replaced by x_i, where the subscripts i,j take the value 1, 2, 3, respectively, a partial derivative with respect to a variable x_i is denoted with ∂_i, and the upper case indices I, $J = 1, \ldots, 6$ indicate the shortened matrix notation where pairs of subscripts (i,j) are replaced by a single number (I or J) according to the correspondence (11) $\rightarrow$ 1, (22) $\rightarrow$ 2, (33) $\rightarrow$ 3, (23) = (32) $\rightarrow$ 4, (13) = (31) $\rightarrow$ 5, (12) = (21) $\rightarrow$ 6. Matrix transposition is denoted by the superscript "$\top$" and complex conjugation by the superscript "$*$".

2. Stress–strain relations

The constitutive equations for anisotropic poroelasticity were introduced by Biot [4,5]. They can be expressed in terms of the microstructural properties as [10]

$$\mathbf{T} = \mathbf{C}^{\mathrm{u}} \cdot \mathbf{S}, \tag{1}$$

where

$$\mathbf{T}^{\top} = (\tau_1, \tau_2, \tau_3, \tau_4, \tau_5, \tau_6, -p), \tag{2}$$

is the stress array, with τ_I the components of the total stress and p the fluid pressure

$$\mathbf{S}^{\top} = (\varepsilon_1, \varepsilon_2, \varepsilon_3, \varepsilon_4, \varepsilon_5, \varepsilon_6, -\zeta), \tag{3}$$

is the strain array, with ε_J ($\varepsilon_J = 2\varepsilon_{ij}$, $i \neq j$) the strain components of the porous frame and ζ the variation of fluid content. The undrained stiffness matrix is given by

$$\mathbf{C}^{\mathrm{u}} = \begin{pmatrix} c_{11}^{\mathrm{u}} & c_{12}^{\mathrm{u}} & c_{13}^{\mathrm{u}} & c_{14}^{\mathrm{u}} & c_{15}^{\mathrm{u}} & c_{16}^{\mathrm{u}} & M\alpha_1 \\ c_{12}^{\mathrm{u}} & c_{22}^{\mathrm{u}} & c_{23}^{\mathrm{u}} & c_{24}^{\mathrm{u}} & c_{25}^{\mathrm{u}} & c_{26}^{\mathrm{u}} & M\alpha_2 \\ c_{13}^{\mathrm{u}} & c_{23}^{\mathrm{u}} & c_{33}^{\mathrm{u}} & c_{34}^{\mathrm{u}} & c_{35}^{\mathrm{u}} & c_{36}^{\mathrm{u}} & M\alpha_3 \\ c_{14}^{\mathrm{u}} & c_{24}^{\mathrm{u}} & c_{34}^{\mathrm{u}} & c_{44}^{\mathrm{u}} & c_{45}^{\mathrm{u}} & c_{46}^{\mathrm{u}} & M\alpha_4 \\ c_{15}^{\mathrm{u}} & c_{25}^{\mathrm{u}} & c_{35}^{\mathrm{u}} & c_{45}^{\mathrm{u}} & c_{55}^{\mathrm{u}} & c_{56}^{\mathrm{u}} & M\alpha_5 \\ c_{16}^{\mathrm{u}} & c_{26}^{\mathrm{u}} & c_{36}^{\mathrm{u}} & c_{46}^{\mathrm{u}} & c_{56}^{\mathrm{u}} & c_{66}^{\mathrm{u}} & M\alpha_6 \\ M\alpha_1 & M\alpha_2 & M\alpha_3 & M\alpha_4 & M\alpha_5 & M\alpha_6 & M \end{pmatrix}, \tag{4}$$

where

$$c_{IJ}^{\mathrm{u}} = c_{IJ} + M\alpha_I\alpha_J \tag{5}$$

(the superscript 'u' denotes undrained), c_{IJ} are the dry-rock stiffness components, M is the fluid/solid coupling modulus and α_I are the effective stress coefficients. The components of the matrix given in Eq. (4) can be expressed in terms of the properties of the frame and of the single constituents (see the appendix).

The variation of fluid content is given by $\zeta = -\mathrm{div}[\phi(\mathbf{u}_{\mathrm{f}} - \mathbf{u})]$, where ϕ is the porosity and $\mathbf{u}_{\mathrm{f}}$ and $\mathbf{u}$ are the average fluid and solid displacements vectors, respectively. The time rate of the strain array can be written as

$$\partial_t \mathbf{S} = \nabla^{\top} \cdot \mathbf{V}, \tag{6}$$

where

$$\mathbf{V} \equiv (v_1, v_2, v_3, q_1, q_2, q_3)^{\top} \tag{7}$$

with v and q denoting the solid and fluid (relative to the solid) particle velocities, respectively [$\mathbf{q} = \phi\partial_t(\mathbf{u}_{\mathrm{f}} - \mathbf{u})$ and $\mathbf{v} = \partial_t\mathbf{u}$], and

$$\nabla = \begin{pmatrix} \partial_1 & 0 & 0 & 0 & \partial_3 & \partial_2 & 0 \\ 0 & \partial_2 & 0 & \partial_3 & 0 & \partial_1 & 0 \\ 0 & 0 & \partial_3 & \partial_2 & \partial_1 & 0 & 0 \\ 0 & 0 & 0 & 0 & 0 & 0 & \partial_1 \\ 0 & 0 & 0 & 0 & 0 & 0 & \partial_2 \\ 0 & 0 & 0 & 0 & 0 & 0 & \partial_3 \end{pmatrix}. \tag{8}$$

Form (6) relating the particle velocities to the strain components, and the differential operator (8) are generalizations of those used by Auld [35].

Biot [5] developed a generalization of the constitutive equations to the viscoelastic case by invoking the correspondence principle and using relaxation functions based on mechanical models of viscoelastic behavior. Viscoelasticity is due to a variety of dissipation mechanisms. One of these mechanisms is the squirt-flow [5,36] by which a force applied to the area of contact between two grains produces a displacement of the surrounding fluid in and out of this area. Since the fluid is viscous, the motion is not instantaneous and energy dissipation occurs. Other important attenuation mechanisms are discussed by Biot [37]. Using the correspondence principle [38], we generalize to relaxation functions the elements of matrix $\mathbf{C}^{\mathrm{u}}$ and Eq. (1) becomes

$$\mathbf{T} = \boldsymbol{\Psi} * \partial_t \mathbf{S}, \tag{9}$$

where $\boldsymbol{\Psi}$ is the relaxation matrix, and "$*$" denotes time convolution and matrix product. Matrix $\mathbf{C}^{\mathrm{u}}$ is obtained from $\boldsymbol{\Psi}$ when $t \to 0$ if we consider that the elastic Biot's poroelastic theory corresponds to the unrelaxed state.

3. Biot–Euler equation

The dynamic equations describing wave propagation in heterogeneous porous media were obtained by Biot [37]. They are

$$\partial_1\tau_1 + \partial_2\tau_6 + \partial_3\tau_5 = \rho\partial_t v_1 + \rho_{\mathrm{f}}\partial_t q_1 + f_1, \tag{10}$$

$$\partial_1\tau_6 + \partial_2\tau_2 + \partial_3\tau_4 = \rho\partial_t v_2 + \rho_{\mathrm{f}}\partial_t q_2 + f_2, \tag{11}$$

$$\partial_1\tau_5 + \partial_2\tau_4 + \partial_3\tau_3 = \rho\partial_t v_3 + \rho_{\mathrm{f}}\partial_t q_3 + f_3, \tag{12}$$

where f denotes body force and $\rho = (1-\phi)\rho_{\mathrm{s}} + \phi\rho_{\mathrm{f}}$ is the composite density, with ρ_{s} and ρ_{f} the solid and fluid densities. On the other hand, the dynamic version of Darcy's law, generalized to the anisotropic case, can be expressed as

$$-\partial_1 p = \rho_{\mathrm{f}}\partial_t v_1 + \psi_1 * \partial_t q_1, \tag{13}$$

$$-\partial_2 p = \rho_{\mathrm{f}}\partial_t v_2 + \psi_2 * \partial_t q_2, \tag{14}$$

$$-\partial_3 p = \rho_{\mathrm{f}}\partial_t v_3 + \psi_3 * \partial_t q_3, \tag{15}$$

where ψ_l, $l = 1, \ldots, 3$ are time-dependent functions related to Biot's viscodynamic effects [37]. In matrix form Eqs. (10)–(15) can be written as

$$\nabla \cdot \mathbf{T} = \mathbf{R} \cdot \partial_t \mathbf{V} + \mathbf{F}, \tag{16}$$

where

$$\mathbf{F} \equiv (f_1, f_2, f_3, 0, 0, 0, 0)^{\top} \tag{17}$$

and

$$\mathbf{R} = \begin{pmatrix} \rho & 0 & 0 & \rho_{\mathrm{f}} & 0 & 0 \\ 0 & \rho & 0 & 0 & \rho_{\mathrm{f}} & 0 \\ 0 & 0 & \rho & 0 & 0 & \rho_{\mathrm{f}} \\ \rho_{\mathrm{f}} & 0 & 0 & \psi_1 * & 0 & 0 \\ 0 & \rho_{\mathrm{f}} & 0 & 0 & \psi_2 * & 0 \\ 0 & 0 & \rho_{\mathrm{f}} & 0 & 0 & \psi_3 * \end{pmatrix}. \tag{18}$$

is the density matrix operator. We refer to (16) as the Biot–Euler equation.

3.1. Time-harmonic fields

Let us consider a time-harmonic field with a time dependence $\exp(\mathrm{i}\omega t)$, where ω is the angular frequency, and $i=\sqrt{-1}$. The stress–strain relation (9) becomes

$$\mathbf{T}=\mathbf{C}\cdot\mathbf{S},\quad \mathbf{C}=\mathscr{F}[\partial_t\mathbf{\Psi}], \tag{19}$$

where $\mathbf{C}$ is the complex and frequency-dependent stiffness matrix, and the operator $\mathscr{F}$ denotes time Fourier transform. Eq. (6) becomes

$$\mathrm{i}\omega\mathbf{S}=\nabla^{\top}\cdot\mathbf{V}. \tag{20}$$

Substituting Eq. (20) into Eq. (19) gives

$$\mathrm{i}\omega\mathbf{T}=\mathbf{C}\cdot(\nabla^{\top}\cdot\mathbf{V}), \tag{21}$$

On the other hand, the Biot–Euler equation (16) becomes

$$\nabla\cdot\mathbf{T}=\mathrm{i}\omega\mathbf{R}\cdot\mathbf{V}+\mathbf{F}, \tag{22}$$

where

$$\mathbf{R}=\begin{pmatrix}\rho & 0 & 0 & \rho_f & 0 & 0\\ 0 & \rho & 0 & 0 & \rho_f & 0\\ 0 & 0 & \rho & 0 & 0 & \rho_f\\ \rho_f & 0 & 0 & Y_1/(\mathrm{i}\omega) & 0 & 0\\ 0 & \rho_f & 0 & 0 & Y_2/(\mathrm{i}\omega) & 0\\ 0 & 0 & \rho_f & 0 & 0 & Y_3/(\mathrm{i}\omega)\end{pmatrix} \tag{23}$$

is the density matrix, and

$$Y_l(\omega)=\mathscr{F}[\partial_t\psi_l], \tag{24}$$

are Biot's viscodynamic operators for the x, y, and z directions. Their explicit form is given in Section 3.3.

3.2. Pore-fluid pressure effects

Let us assume a rock—a sandstone or a limestone—at depth z. The lithostatic pressure p_c for an average sediment density $\bar{\rho}$ is equal to $p_c=\bar{\rho}gz$, where g is the acceleration of gravity. On the other hand, the hydrostatic pore pressure is approximately $p_H=\bar{\rho}_w gz$, where ρ_w is the density of water.

3.2.1. Stiffness and porosity versus pressure

A proper analysis of the dependence of wave properties on pore pressure and confining stress in anisotropic media requires a complete experimental data set, i.e. dry-rock velocity measurements versus confining stress, and wet-rock velocity measurements versus pore pressure and confining stress. These data are necessary to calculate the effective stress coefficients [39]. A complete data set for anisotropic media is, to our knowledge, not yet available in the literature.

Hooke's law (1) for anisotropic poroelastic media can be rewritten as [10]

$$\tau_I=c_{IJ}\varepsilon_J-\alpha_I p,\quad I,J=1,\ldots,6. \tag{25}$$

In this context, the effective stress is given by $\tau_{eI}=c_{IJ}\varepsilon_J$, such as

$$\tau_{eI}=\tau_I+\alpha_I p. \tag{26}$$

The total stress is decomposed into an effective stress, which acts on the frame, and into a hydrostatic stress, which acts on the fluid. The effective-stress concept means that the response of the saturated porous medium is described by the response of the dry porous medium with the applied stress replaced by the effective stress.

The problem to establish an effective stress law for the anisotropic case is that an hydrostatic loading does not compensate the variations in pore pressure to keep the dry-rock moduli unchanged. For instance, two different confining pressure should be associated with c_{11} and c_{33}. The problem resides in determining the ratio between these two confining pressures and, in general, the pressures associated with the other elastic moduli. Experiments are required to establish the proper effective stress law. In the isotropic case, the dry-rock bulk modulus can be shown to depend only on the differential pressure $p_d=p_c-p_H$ [31,20]. An approximation is to use a single pressure for all moduli, and interpret this pressure as a mean pressure. We assume the same dependence for the dry-rock elastic constants and density. We consider the following functional form for these constants and the density as a function of confining pressure:

$$c_{IJ}=c_0+c_1p_c+c_2\exp(-c_3p_c), \tag{27}$$

$$\rho=r_0+r_1p_c+r_2\exp(-r_3p_c), \tag{28}$$

where c_k and r_k, $k=1,\ldots,3$, are coefficients obtained by fitting the experimental data. Then, the elastic constants and density of the frame versus pore and confining pressures are obtained from Eqs. (27) and (28) by substituting p_c with p_d, and the wet-rock complex stiffness constants are obtained from the stress–strain relation (19).

Changes in porosity are not as important as changes in stiffness. In this sense, porosity-based methods can be highly unreliable. In fact, for changes of the confining pressure from 0 to 100 MPa, the changes in the porosity of Navajo sandstone, Weber sandstone and Berea sandstone are only 1.7%, 7% and 4.5%, respectively, [40]. High pore pressure implies opening of microcracks (compliant pores), and this has a greater influence on the stiffnesses than on the porosity. We assume that the effective stress coefficient for porosity is equal to 1 [31,40].

3.2.2. Permeability and viscosity versus pressure

The permeability considered in the viscodynamic dissipation (see next section) is the global permeability, i.e., that related to the connected pores and cracks. Pressure effects are more pronounced in rocks where permeability is due to fractures. The effects are small for stiff pores between spherical grains. The porosity at grain contacts in sandstones can be viewed as a fracture porosity. Thus, the effects can be large or small depending on whether these contacts maintain interconnectivity of the pore network [41].

The permeability can be obtained from the classical Kozeny–Carman relation. For a packing of spheres and cylindrical pores, the eigenvalues of the permeability tensor in its natural coordinate system can be expressed by [41,42]

$$\kappa_l = \frac{B_l(\phi-\phi_\mathrm{p})^3}{(1-\phi+\phi_\mathrm{p})^2}, \quad l=1,\ldots,3, \tag{29}$$

where the coefficients B_l and ϕ depend on pore and confining pressure. Following Mavko and Nur [43], we have introduced a percolation porosity, ϕ_p.

Gangi [44] obtained an empirical relation between permeability and confining pressure:

$$B_l(p_\mathrm{c}) = B_{l0}\left[1-\left(\frac{p_\mathrm{c}}{p_1}\right)^m\right]^3, \tag{30}$$

where m, B_{l0} and p_1 are constants. We define the effective stress as the confining pressure that would give the same value of κ_l: $\kappa_l(p_\mathrm{e}, p=0)=\kappa(p_\mathrm{c},p)$. In the case of transverse isotropy, discussed in the previous section, we use the effective stress coefficient [40]

$$n_\kappa = 1-\frac{\phi(1-\alpha)}{6(\alpha-\phi)+\phi}, \tag{31}$$

where $\alpha=(2\alpha_1+\alpha_3)/3$. Using the effective pressure $p_\mathrm{e}=p_\mathrm{c}-n_\kappa p$, we substitute p_c by p_e in Eq. (30) to obtain

$$B_l(p_\mathrm{c}) = B_{l0}\left[1-\left(\frac{p_\mathrm{e}}{p_1}\right)^m\right]^3. \tag{32}$$

We assume that the viscosity of water is independent of pressure. For the gas viscosity η_g we assume the equation proposed by Luo and Vasseur [29]. It depends on pore pressure and temperature T:

$$\eta_\mathrm{g}[\mathrm{Pa\,s}] = 10^{-5}+1.5\times10^{-8}\frac{p}{\bar{\rho}g} - 2.2\times10^{-7}(T-T_0), \tag{33}$$

where T_0 is the surface temperature.

3.3. Viscodynamic and stiffness attenuation

Attenuation can be related to the strain energy (stiffness dissipation) and the kinetic energy (viscodynamic dissipation). In natural porous media such as sandstones, wave dissipation is due to complex pore shapes and to the presence of clay. This complexity gives rise to a variety of relaxation mechanisms. Stoll and Bryan [45] show that attenuation is controlled by both the anelasticity of the skeleton (friction at grain contacts) and by viscodynamic causes. Stiffness dissipation is described in the stress–strain relation, and viscodynamic dissipation is a dynamic permeability effect due to the frequency-dependent interaction between the pore fluid and the solid matrix [26].

In the low-frequency range [37,46], i.e., for frequencies lower than $\omega_\mathrm{c}=\min(\omega_l)$, where $\omega_l=\eta/(m_l\kappa_l)$, one has

$$\psi_l(t) = m_l\delta(t)+\frac{\eta}{\kappa_l}H(t), \tag{34}$$

where $m_l=\mathscr{T}_l\rho_\mathrm{f}/\phi$, with $\mathscr{T}_l$ the tortuosity, η is the dynamic viscosity, κ_l $(l=1,2,3)$ are the principal components of the permeability tensor, $\delta(t)$ is Dirac's function, and $H(t)$ is the Heaviside function. From Eq. (24),

$$Y_l(\omega) = \mathrm{i}\omega m_l+\frac{\eta}{\kappa_l}. \tag{35}$$

In terms of mechanical models, Eq. (35) represents a Kelvin–Voigt element [38].

In the high-frequency range ($\omega\geqslant\omega_\mathrm{c}$), the viscodynamic operator is strongly influenced by the pore geometry, and a precise evaluation of its frequency dependence requires an experimental determination [46]. Johnson et al. [26] obtained an expression for the viscodynamic function, which provides a good description of both the magnitude and phase of the exact dynamic tortuosity of large networks formed from a distribution of random radii. The viscodynamic function are

$$F_l(\omega) = \sqrt{1-\frac{4\mathrm{i}\mathscr{T}_l^2\kappa_l}{x_l\Lambda_l^2\phi}}, \quad x_l=\frac{\eta\phi}{\omega\kappa_l\rho_\mathrm{f}}, \quad l=1,\ldots,3, \tag{36}$$

where Λ_l is a geometrical, and Λ_l is a geometrical parameter, with $2/\Lambda_l$ being the surface-to-pore volume ratio of the pore–solid interface. The following relation between $\mathscr{T}_l$, κ_l, and Λ_l can be used: $\xi_l\mathscr{T}_l\kappa_i/\phi\Lambda_l^2=1$; where ξ_l describes the shape of the pore network $\xi_l=12$ for a set of oblique slabs of fluid, and $\xi_l=8$ for a set of non-intersecting oblique tubes. The new viscodynamic components are

$$Y_l(\omega) = \mathrm{i}\omega m_l+\frac{\eta F_l(\omega)}{\kappa_l}. \tag{37}$$

Tortuosity is assumed to be independent of confining and pore pressures.

The description of viscoelastic dissipation is phenomenological. Constant-Q models provide a simple parameterization of seismic attenuation in rocks. By reducing the number of parameters they allow an improvement of seismic inversion. Moreover, there is

physical evidence that attenuation is almost linear with frequency (therefore Q is constant) over many octaves. Bland [47] and Kjartansson [23] discuss a linear attenuation model with the required characteristics, but the idea is much older (see, e.g. [48]).

The attenuation kernels corresponding to a Q independent of frequency are

$$M_l(\omega, Q_l) = \left(\frac{\mathrm{i}\omega}{\omega_0}\right)^{2\gamma_l},$$
$$\gamma_l = \frac{1}{\pi}\tan^{-1}\left(\frac{1}{Q_l}\right), \quad l = 1, \ldots 6, \tag{38}$$

where Q_l is the quality factor and ω_0 is a reference frequency. Attenuation is modeled by making complex and frequency dependent the eigenstiffnesses of the elasticity matrix (4), according to the theory developed by Carcione and Cavallini [49]. The method is illustrated in Section 5.

3.4. Partial saturation effects

The composite properties of the mixture hydrocarbon/water depend on the relative concentrations and on the properties of the constituents. They are

$$K_\mathrm{f} = (S_\mathrm{g}K_\mathrm{g}^{-1} + S_\mathrm{w}K_\mathrm{w}^{-1})^{-1} \tag{39}$$

(Reuss's model) and

$$\rho_\mathrm{f} = S_\mathrm{g}\rho_\mathrm{g} + S_\mathrm{w}\rho_\mathrm{w}, \tag{40}$$

where K_g and K_w are the bulk moduli of the hydrocarbon and water, respectively, and ρ_g is the density of the hydrocarbon. We assume that the fluid viscosity is given by [50]

$$\eta = \eta_\mathrm{g}\left(\frac{\eta_\mathrm{w}}{\eta_\mathrm{g}}\right)^{S_\mathrm{w}}, \tag{41}$$

where η_g and η_w are the viscosities of the hydrocarbon and water, respectively. Eq. (41) is a good approximation for most values of the saturations.

Eq. (39) corresponds to the low-frequency range. When the fluids are not mixed in the pore volume, but distributed in patches, the effective bulk modulus of the fluid at high frequencies is higher than that predicted by Eq. (39). We use an empirical mixing equation introduced by Brie et al. [34]. The effective fluid bulk modulus is given by

$$K_\mathrm{f} = (K_\mathrm{w} - K_\mathrm{g})(S_\mathrm{w})^\beta + K_\mathrm{g}, \tag{42}$$

where $\beta = (f_0/f)^{0.34}$ is an empirical parameter, with f_0 being a reference frequency ($f_0 = 1$ MHz in the example). The exponent 0.34 fits data from the seismic to the ultrasonic band, particularly the sonic-band values provided by Brie et al. [34]. Eq. (42) gives Voigt's mixing law for $\beta = 1$ and a good approximation of Reuss's model for $\beta = 40$.

The gas density and bulk modulus as a function of pressure and temperature are calculated using the van der Waals equation [51]. We assume a constant sediment burial rate, b, and a constant geothermal gradient, G. Hence, the temperature variation of a particular sediment volume is

$$T = T_0 + Gz, \quad z = bt \tag{43}$$

with t is deposition time. Typical values of G range from 10 to 30°C/km, while b may range between 0.05 and 3 km/m.y. (m.y. = million years) [52].

For an anisotropic porous medium, each of the permeability components κ_l may have a different functional relationship to S_w. Hence, use of the relative permeability concept is not permitted [53,54]. Because there are no experimental data (Bear, personal communication), we assume an ad hoc relation between those components, based on the following qualitative observation in rocks saturated with water and gas. Let us assume transverse isotropy and $\kappa_1 > \kappa_3$ at full water saturation, due to pore cross sections which are larger in the x direction. As water saturation is reduced, and the larger pores drained first, a saturation is reached at which $\kappa_1 = \kappa_3$. Then, as saturation is further reduced, $\kappa_1 < \kappa_3$. At the other end (full gas saturation), we again have $\kappa_1 > \kappa_3$. This behavior can be modeled with the following relations between permeability and saturation:

$$B_{10} = b_1[1 - (1 - 0.3a)\sin(\pi S_\mathrm{w})] \tag{44}$$

and

$$B_{30} = ab_1[1 - 0.5\sin(\pi S_\mathrm{w})] \tag{45}$$

(see Eq. (32)), where b_1 is a constant and a is a permeability-anisotropy parameter. Note that for $S_\mathrm{w} = 0$ or 1, $B_{30}/B_{10} = a$. Eqs. (44) and (45) are purely hypothetical and serve for the example illustrated in Section 5 to model the qualitative behavior mentioned above. Those equations model the rotation of the ellipses of directional permeability versus saturation obtained by Bear et al. [54] by means of numerical experiments.

4. Expression of measurable quantities

For homogeneous waves, the propagation and attenuation directions coincide, and the complex wavevector can be written as

$$\mathbf{k} = (\kappa - \mathrm{i}\alpha)\hat{\boldsymbol{\kappa}} \equiv k\hat{\boldsymbol{\kappa}}, \tag{46}$$

where k is the complex wavenumber, κ is the real wavenumber, α is the attenuation factor, and

$$\hat{\boldsymbol{\kappa}} = (l_1, l_2, l_3) \tag{47}$$

defines the propagation direction through the directions cosines l_1, l_2 and l_3.

The Christoffel equation is [20]

$$(\mathbf{R}^{-1}\cdot\boldsymbol{\Gamma}-V^2\mathbf{I}_6)\cdot\mathbf{V}=0, \tag{48}$$

where

$$\boldsymbol{\Gamma}=\mathbf{L}\cdot\mathbf{C}\cdot\mathbf{L}^{\top} \tag{49}$$

is the Christoffel matrix,

$$V=\omega/k \tag{50}$$

is the complex velocity,

$$\mathbf{L}=\begin{pmatrix} l_1 & 0 & 0 & 0 & l_3 & l_2 & 0\\ 0 & l_2 & 0 & l_3 & 0 & l_1 & 0\\ 0 & 0 & l_3 & l_2 & l_1 & 0 & 0\\ 0 & 0 & 0 & 0 & 0 & 0 & l_1\\ 0 & 0 & 0 & 0 & 0 & 0 & l_2\\ 0 & 0 & 0 & 0 & 0 & 0 & l_3 \end{pmatrix}, \tag{51}$$

and $\mathbf{I}_6$ denotes the six-dimensional unit matrix.

Making the determinant zero, Eq. (48) gives the following dispersion relation:

$$\det(\mathbf{R}^{-1}\cdot\boldsymbol{\Gamma}-V^2\mathbf{I}_6)=0. \tag{52}$$

The eigensystem formed by Eqs. (48) and (52) gives six eigenvalues and their corresponding eigenvectors. Four of them correspond to the wave modes, and the others equal zero. These modes correspond to the fast and slow quasi-compressional waves, and the two quasi-shear waves. Matrix $\boldsymbol{\Gamma}$ has therefore rank four, despite its 6×6 dimension. Three of the rows are linearly dependent, and this is somehow related to the space dimension.

The slowness and attenuation vectors for homogeneous waves can be expressed in terms of the complex velocity as

$$\mathbf{s}=\mathrm{Re}\left(\frac{1}{V}\right)\hat{\boldsymbol{\kappa}} \tag{53}$$

and

$$\boldsymbol{\alpha}=-\omega\,\mathrm{Im}\left(\frac{1}{V}\right)\hat{\boldsymbol{\kappa}}, \tag{54}$$

respectively [$(1/V)$ is the reciprocal of the phase velocity].

Following Carcione [20], the time-average kinetic energy density is

$$\langle K\rangle=\frac{1}{4}\mathrm{Re}(\mathbf{V}^{*\top}\cdot\mathbf{R}\cdot\mathbf{V}) \tag{55}$$

and the time-average strain energy density is

$$\langle S\rangle=\frac{1}{4}|V|^{-2}\mathrm{Re}(V^2\mathbf{V}^{\top}\cdot\mathbf{R}\cdot\mathbf{V}^{*}), \tag{56}$$

where $\mathbf{V}$ are the eigenvectors of $\mathbf{R}^{-1}\cdot\boldsymbol{\Gamma}$. Eq. (56) is formally similar to the strain energy density in single-phase anisotropic-viscoelastic media, where $\langle S\rangle=\frac{1}{4}\rho_s|V|^{-2}V^2|\mathbf{V}|^2$ [2]. In the single-phase medium, every particle velocity component is equally weighted by the density. Note that, when the medium is lossless, V is real and the strain energy density equals the kinetic energy density.

The stored energy density is then

$$\langle E\rangle=\frac{1}{4}\mathrm{Re}\left[\left(1+\frac{V^2}{|V|^2}\right)\mathbf{V}^{\top}\cdot\mathbf{R}\cdot\mathbf{V}^{*}\right]. \tag{57}$$

When the medium is lossless, V and $\mathbf{R}$ are real, and $\langle E\rangle$ is equal to twice the average kinetic energy (55).

The average power flow can be written as

$$\langle\mathbf{P}\rangle=\frac{1}{2}\mathrm{Re}[V^{-1}\mathbf{V}^{\top}\cdot\mathbf{L}\cdot\mathbf{C}\cdot(\hat{\mathbf{e}}_i\mathbf{U}^{i^{\top}})\cdot\mathbf{V}^{*}], \tag{58}$$

where $\hat{\mathbf{e}}_i$ is the unit Cartesian vector and the Einstein convention for repeated indices is used; $\mathbf{U}^i$ are 6×7 matrices with most of their elements equal to zero, except U^1_{11}, U^1_{26}, U^1_{35}, U^1_{47}, U^2_{16}, U^2_{22}, U^2_{34}, U^2_{57}, U^3_{15}, U^3_{24}, U^3_{33} and U^3_{67}, which are equal to 1.

The wave surface is the locus of all endpoints of the energy velocity vectors (it is a surface in velocity space). The wavefront generated by a point source (a surface in location space) at time t is the locus of the endpoints of all location vectors obtained by multiplying all energy velocity vectors with t. The energy velocity is defined as the ratio of the average power flow density $\langle\mathbf{P}\rangle$ to the total energy density $\langle E\rangle$. Since this is equal to the sum of the average kinetic and strain energy densities $\langle K\rangle$ and $\langle S\rangle$, the energy velocity is

$$\mathbf{V}_e=\frac{\langle\mathbf{P}\rangle}{\langle K+S\rangle}. \tag{59}$$

The dissipated energy can be expressed as

$$\langle D\rangle=\frac{1}{2}\mathrm{Im}\left[\left(-1+\frac{V^2}{|V|^2}\right)\mathbf{V}^{\top}\cdot\mathbf{R}\cdot\mathbf{V}^{*}\right]. \tag{60}$$

The quality factor for homogeneous waves is

$$Q=\frac{2\langle S\rangle}{\langle D\rangle}=\frac{\mathrm{Re}(V^2\mathbf{V}^{\top}\cdot\mathbf{R}\cdot\mathbf{V}^{*})}{2\,\mathrm{Im}(V)\mathrm{Re}(V\mathbf{V}^{\top}\cdot\mathrm{R}\cdot\mathbf{V}^{*})}. \tag{61}$$

If there are no losses due to viscosity effects ($\mathbf{R}$ is real), $\mathbf{V}^{\top}\cdot\mathbf{R}\cdot\mathbf{V}^{*}$ is real and

$$Q=\frac{\mathrm{Re}(V^2)}{\mathrm{Im}(V^2)}, \tag{62}$$

as in the single-phase case [2].

5. Example

We consider the dry-rock measurements in transversely isotropic Berea sandstone obtained by Lo et al. [11]. (Dry-rock stiffnesses can also be obtained from anisotropic models of cracked rocks [55–57].) Although Lo et al.'s data do not reflect the situation at depth, since the experiments are ultrasonic measurements, we assume that at seismic frequencies their sample corresponds to a fractured formation, and that the effective medium assumption is valid from the seismic range to

the ultrasonic frequency range. As long as the anisotropy of elasticity and that of permeability have the same cause, they must have some symmetry elements in common. Since the permeability tensor is of rank two and the elasticity tensor is of rank four, the symmetry of permeability must be a subset of the symmetry of elasticity. In the case of anisotropy caused by fractures, the principal directions of the permeability tensor coincide with the corresponding axes of the elasticity tensor, but this may not be the case in other rocks [13]. Note that the forms (18) and (23) of the density matrix imply that the permeability tensor is expressed in its principal coordinate system, but the elasticity matrix (4) has not such restriction.

Fig. 1 shows the best-fit curves to the dry-rock elastic constants (a), density (b), and porosity (c) versus confining pressure p_c. We get

$$
\begin{aligned}
c_{11} &= 32.74 + 0.043p_c - 9.97\exp(-0.06p_c),\\
c_{33} &= 31.87 + 0.035p_c - 14.59\exp(-0.056p_c),\\
c_{44} &= 14.93 + 0.011p_c - 5.58\exp(-0.053p_c),\\
c_{12} &= 3.06 + 0.01p_c - 0.26\exp(-0.25p_c),\\
c_{13} &= 4.68 - 0.015p_c - 1.7\exp(-0.036p_c),\\
\rho &= 2.1441 + 0.00038p_c - 0.045\exp(-0.0226p_c),\\
\phi &= 1 - \rho/\rho_s, \qquad (63)
\end{aligned}
$$

where the elastic constants are given in GPa, the density in g/cm^3 and the confining pressure in MPa. Note that, knowing the grain density ρ_s, we can estimate porosity versus confining pressure, because $\rho = (1-\phi)\rho_s$ for the dry rock (assuming that ρ_s is pressure independent). For quartz, $\rho_s = 2.65$ g/cm^3, and $\phi = 17\%$ at 5 MPa and $\phi = 15\%$ at 100 MPa. Hence, changes in porosity are not very significant.

Polar representations of the dry-rock energy velocities are shown in Figs. 2a and b for $p_c = 0$ MPa and 100 MPa, respectively. The curves correspond to a plane perpendicular to the plane of isotropy. Only one quarter of the curves are displayed, because of symmetry. The tick marks indicate the polarization directions, with the points uniformly sampled as a function of the phase angle. Note that, as expected, the deviations from isotropy is stronger at zero confining pressure.

Let us consider the presence of fluid, and obtain the acoustic properties as a function of pore pressures and saturation. We assume 3 km depth. If the average sediment density is 2.4 g/cm^3, the confining pressure is $p_c = 70.6$ MPa and the hydrostatic pressure is $p_H = 30.6$ MPa (assuming $\rho_w = 1040$ kg/m^3). With a surface temperature of 25°C and a geothermal gradient $G = 25$°C/km, $T = 100$°C. We assume that the rock is saturated with water and gas. The properties of water are assumed pressure independent. Water properties are $K_w = 2.5$ GPa, $\rho_w = 1040$ kg/m^3 and $\eta_w = 1$ cP, while

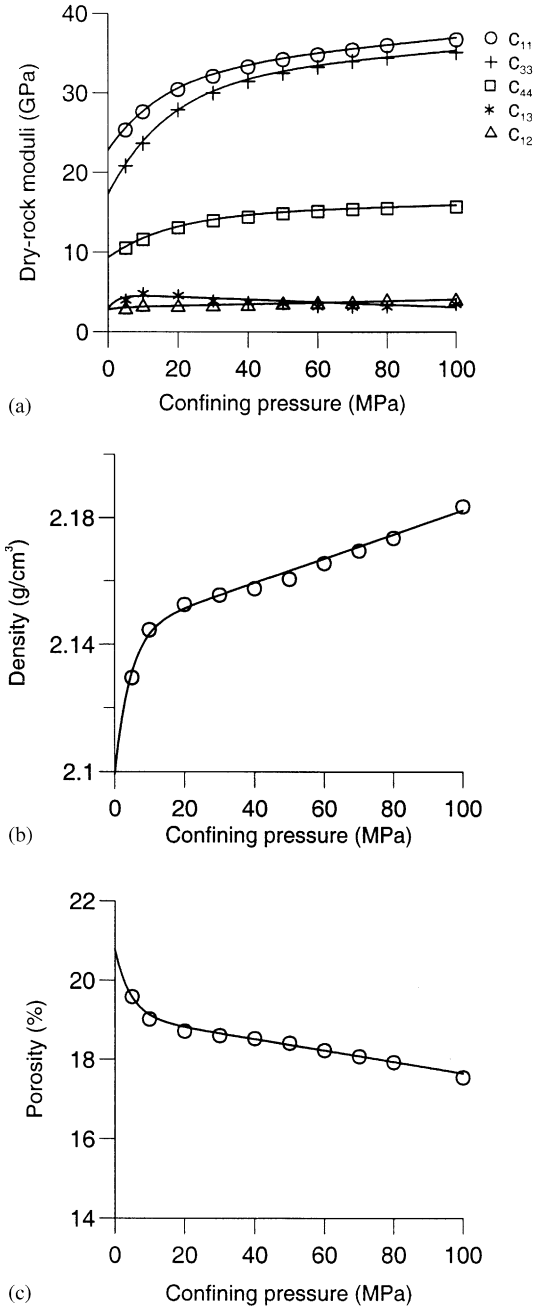

Fig. 1. Best-fit curves to the dry-rock elastic constants (a), density (b) and porosity (c) of Berea sandstone versus confining pressure p_c. The experimental data are from Lo et al. [11].

gas properties at hydrostatic pressure are $K_g = 0.059$ GPa, $\rho_g = 116$ kg/m^3 and $\eta_g = 0.013$ cP. The grain bulk modulus is $K_s = 39$ GPa, the grain density is $\rho_s = 2650$ kg/m^3, and the tortuosites are $\mathscr{T}_1 = \mathscr{T}_2 = 2$ and $\mathscr{T}_3 = 5$. The parameters involved in the permeability expressions are $\phi_p = 0.04, m = 0.26, p_1 = 10$ GPa, $b_1 = 6\times10^{-11}$ m^2, and $a = 0.2$. Fig. 3 shows the permeability components versus confining pressure (a) (at full water saturation), and saturation (b) (at hydrostatic pressure).

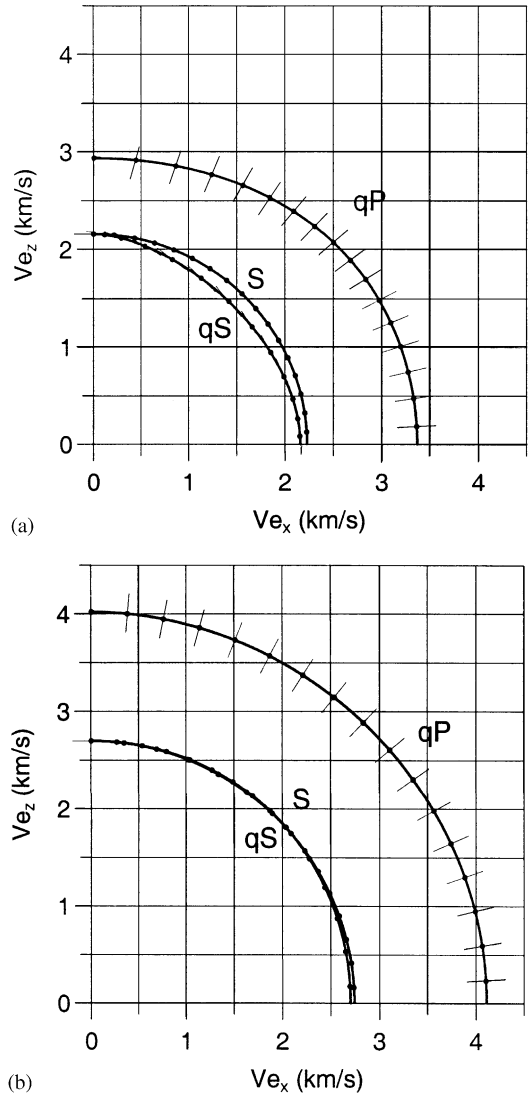

Fig. 2. Polar representations of the dry-rock energy velocities for $p_c = 0$ MPa (a) and $p_c = 100$ MPa (b). qP is the quasi-compressional wave, qS is the quasi-shear wave and S is the cross-plane shear wave. The curves correspond to a plane perpendicular to the plane of isotropy. Only one-quarter of the curves are displayed because of symmetry. The tick marks indicate the polarization directions.

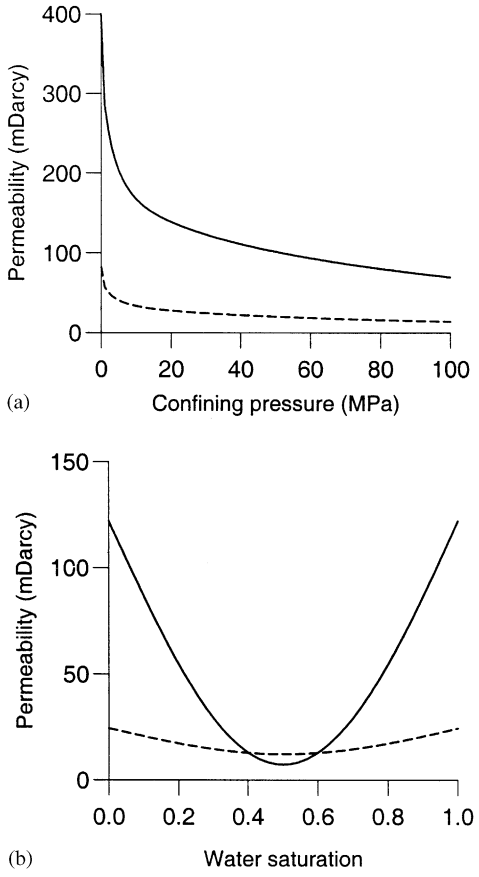

Fig. 3. Permeability components versus pressure, at full water saturation (a), and versus water saturation, at hydrostatic pressure (b). The solid and dashed lines correspond to κ_1 and κ_3, respectively.

To introduce viscoelastic attenuation, we use a constitutive equation based on the fact that each eigenvector (called eigenstrain) of the stiffness matrix defines a fundamental deformation state of the medium. The six eigenvalues (called eigenstiffnesses) represent the intrinsic elastic parameters. In the elastic case the strain energy is uniquely parameterized by the six eigenstiffnesses. These ideas date back to the middle of the 19th century when Lord Kelvin introduced the concept of "principal strain" (eigenstrain in modern terminology) to describe the deformation state of a medium [58]. From this fact and the correspondence principle, Carcione and Cavallini [49] inferred that in a real medium the rheological properties depend essentially on six relaxation functions, which are the generalization of the eigenstiffnesses to the viscoelastic case. The existence of six or fewer complex moduli depends on the symmetry class of the medium.

Let us illustrate the method to model stiffness (or viscoelastic) attenuation for a pore pressure of 68 MPa, full water saturation and $f = 25$ Hz. According to Eqs. (63), the stiffness matrix of the drained porous medium (c_{IJ}; see the Appendix A) in Voigt notation is

$$\begin{pmatrix} 31.8 & 3.34 & 4.28 & 0 & 0 & 0 \\ 3.34 & 31.8 & 4.28 & 0 & 0 & 0 \\ 4.28 & 4.28 & 29.4 & 0 & 0 & 0 \\ 0 & 0 & 0 & 13.8 & 0 & 0 \\ 0 & 0 & 0 & 0 & 13.8 & 0 \\ 0 & 0 & 0 & 0 & 0 & 14.2 \end{pmatrix},$$

in GPA. They are used to calculate the elements of matrix $\mathbf{C}^{\mathrm{u}}$, which correspond to the high-frequency

(unrelaxed) limit. It gives

$$\mathbf{C}^{\mathrm{u}} = \begin{pmatrix} 36.9 & 8.43 & 9.46 & 0 & 0 & 0 & 7.67 \\ 8.43 & 36.9 & 9.46 & 0 & 0 & 0 & 7.67 \\ 9.46 & 9.46 & 34.7 & 0 & 0 & 0 & 7.81 \\ 0 & 0 & 0 & 13.8 & 0 & 0 & 0 \\ 0 & 0 & 0 & 0 & 13.8 & 0 & 0 \\ 0 & 0 & 0 & 0 & 0 & 14.2 & 0 \\ 7.67 & 7.67 & 7.81 & 0 & 0 & 0 & 11.6 \end{pmatrix},$$

in GPa. In order to apply Kelvin's formulation, Hooke's law has to be written in tensorial form. This implies multiplying the Eqs. (44), (55) and (66) elements of matrix $\mathbf{C}^{\mathrm{u}}$ by a factor 2 [49] and taking the leading principal submatrix of order 6 (the upper-left 6×6 matrix). This can be done for the undrained porous medium, for which the variation of fluid content ζ is equal to zero (closed system). Let us call this new 6×6 matrix (tensor) $\bar{\mathbf{C}}^{\mathrm{u}}$. This matrix can be diagonalized to obtain

$$\bar{\mathbf{C}}^{\mathrm{u}} = \mathbf{A} \cdot \mathbf{\Lambda} \cdot \mathbf{A}^{\top}, \tag{64}$$

where $\mathbf{\Lambda} = \mathrm{diag}(\lambda_1, \lambda_2, \lambda_3, \lambda_4, \lambda_5, \lambda_6)^{\top}$ is the eigenvalue matrix, and $\mathbf{A}$ is the matrix formed with the eigenvectors of $\bar{\mathbf{C}}^{\mathrm{u}}$, or more precisely, with the columns of the right (orthonormal) eigenvectors (note that the symmetry of $\bar{\mathbf{C}}^{\mathrm{u}}$ implies $\mathbf{A}^{-1} = \mathbf{A}^{\top}$). The eigenstiffnesses are $\Lambda_1 = 54.4$ GPa, $\Lambda_2 = \Lambda_3 = 28.4$ GPa, $\Lambda_4 = \Lambda_5 = 27.6$ GPa, and $\Lambda_6 = 25.6$ GPa.

In virtue of the correspondence principle and its application to Eq. (64) we introduce the viscoelastic stiffness tensor

$$\bar{\mathbf{C}} = \mathbf{A} \cdot \mathbf{\Lambda}^{(\mathrm{v})} \cdot \mathbf{A}^{\top}, \tag{65}$$

where $\mathbf{\Lambda}^{(\mathrm{v})}$ is a diagonal matrix with entries

$$\lambda_I^{(\mathrm{v})}(\omega) = \lambda_I M_I(\omega), \quad I = 1, \ldots, 6. \tag{66}$$

The quantities M_I are complex and frequency-dependent dimensionless moduli, given by Eq. (38). A quality

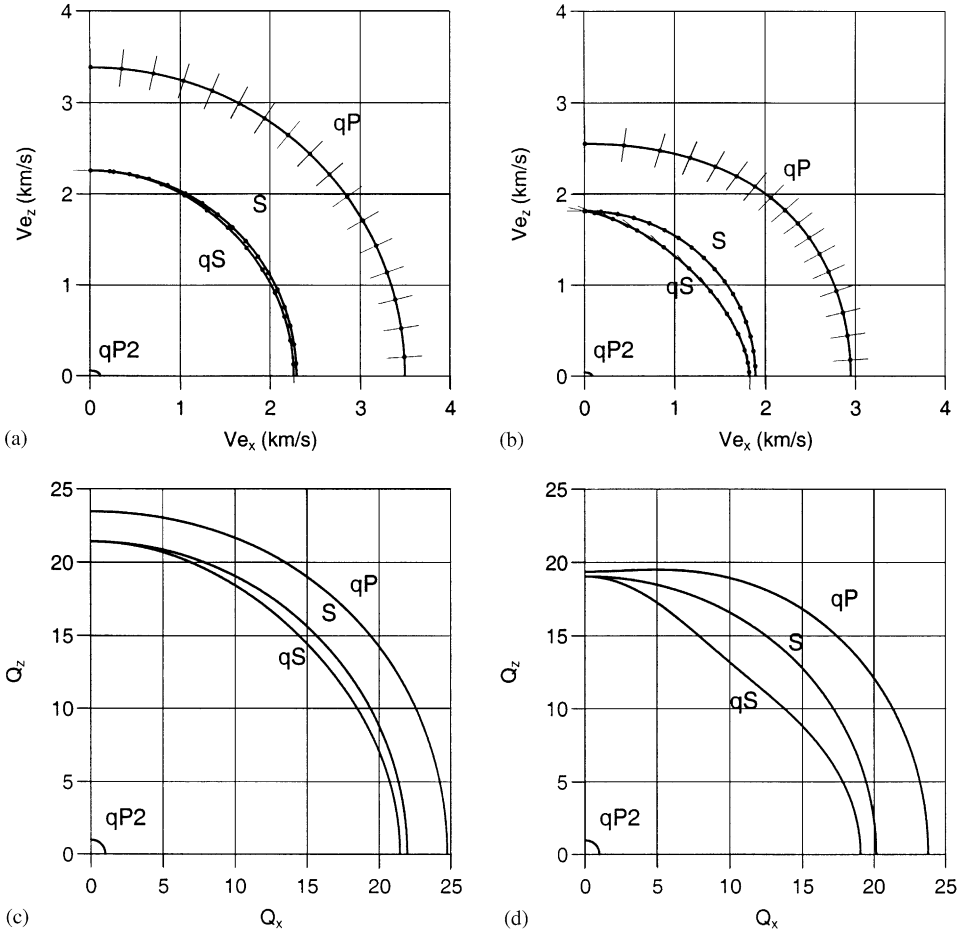

Fig. 4. Polar representations of the wet-rock energy velocities and quality factors for $p = p_{\mathrm{H}}$ (a and c) and $p = 68$ MPa (b and d), with $S_{\mathrm{w}} = 15\%$ and $f = 25$ Hz.

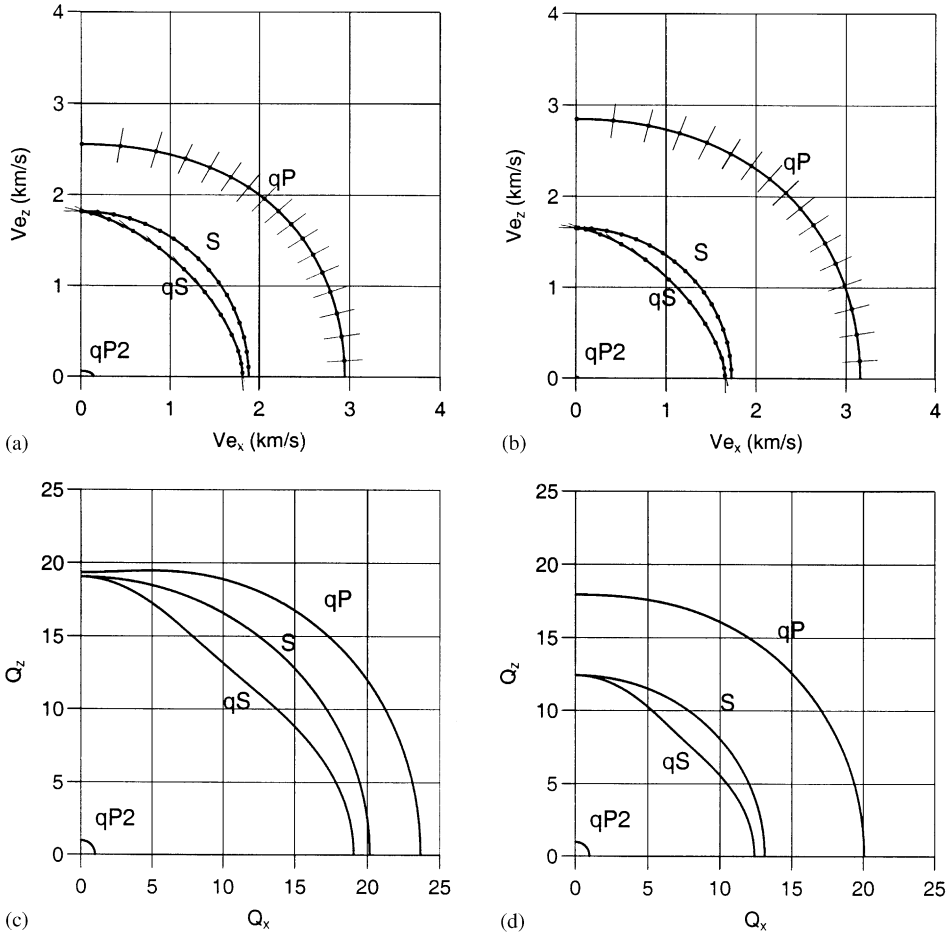

Fig. 5. Polar representations of the wet-rock energy velocities and quality factors for $S_w = 0$ (a and c) and $S_w = 100\%$ (b and d), with $p = 68$ MPa and $f = 25$ Hz.

factor Q_I is assigned to each modulus M_I. To recover Voigt's notation, we should divide Eqs. (44), (55) and (66) elements of matrix $\bar{\mathbf{C}}$ by a factor 2. This gives the complex matrix $\mathbf{C}$.

In transversely isotropic porous media there are five distinct eigenvalues, and therefore five complex moduli (see Carcione and Cavallini [49] for the single-phase case). We assume that the dimensionless quality factors are defined as $Q_I = (\lambda_I/\lambda_1)Q_1$, $I = 1, \ldots, 6$, where Q_1 corresponds to the quasi-dilatational mode. Let us consider $Q_1 = Q_0 = 30$ (for all cases) and $\omega_0 = 1$ MHz, such that

$$Q_1 = \left[\frac{\Lambda_1(z,p)}{\Lambda_1(z,p_H)}\right] Q_0. \tag{67}$$

This choice implies that the higher the stiffness, the higher the quality factor (i.e., the harder the medium, the lower the attenuation), and that attenuation increases with increasing pore pressure. Then, matrix $\mathbf{C}$ is given by

$$\begin{pmatrix}
26.6 + \mathrm{i}1.26 & 8.11 + \mathrm{i}0.008 & 9.06 + \mathrm{i}0.1 & \\
8.11 + \mathrm{i}0.008 & 26.6 + \mathrm{i}1.26 & 9.06 + \mathrm{i}0.1 & \\
9.06 + \mathrm{i}0.1 & 9.06 + \mathrm{i}0.1 & 24.6 + \mathrm{i}1.22 & \\
0 & 0 & 0 & \\
0 & 0 & 0 & \\
0 & 0 & 0 & \\
7.67 & 7.67 & 7.81 & \\
0 & 0 & 0 & 7.67 \\
0 & 0 & 0 & 7.67 \\
0 & 0 & 0 & 7.81 \\
8.86 + \mathrm{i}0.58 & 0 & 0 & 0 \\
0 & 8.86 + \mathrm{i}0.58 & 0 & 0 \\
0 & 0 & 9.24 + \mathrm{i}0.59 & 0 \\
0 & 0 & 0 & 11.6
\end{pmatrix},$$

in GPa.

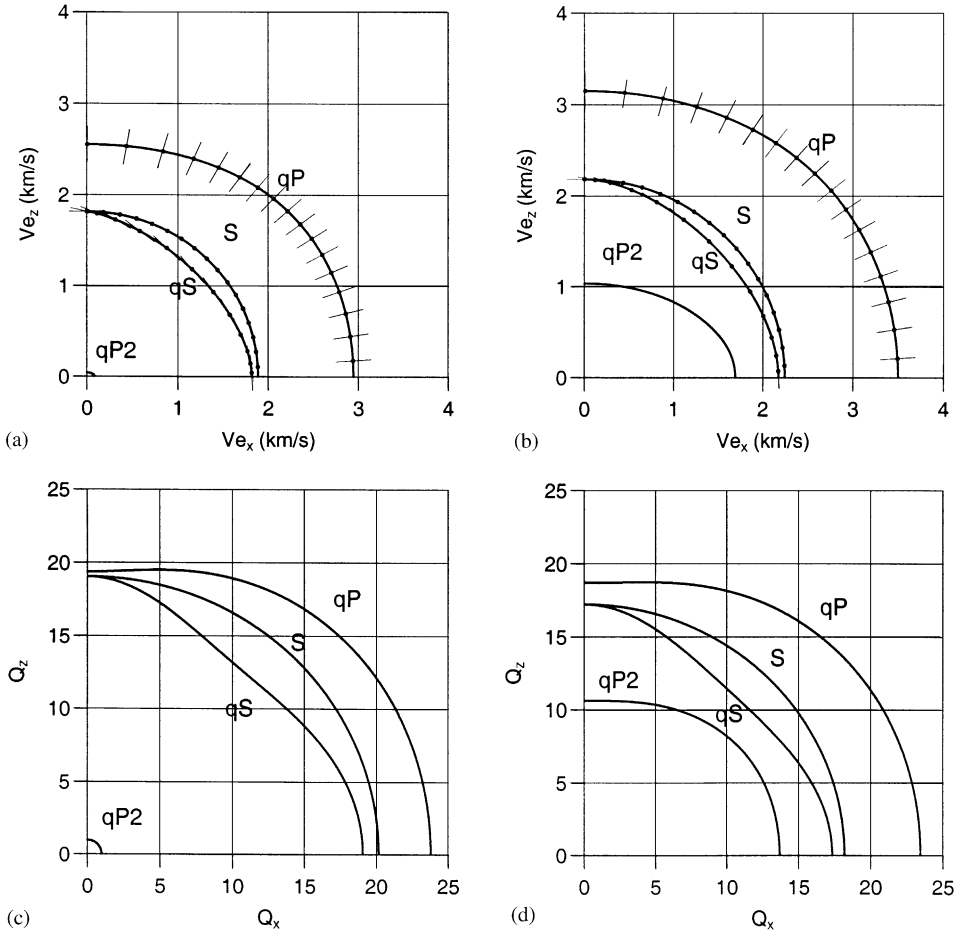

Fig. 6. Polar representations of the wet-rock energy velocities and quality factors for $f = 25$ Hz (a and c) and $f = 1$ MHz (b and d), with $p = 68$ MPa and $S_w = 15\%$.

We consider three cases: (i) $p = p_H$ and $p = 68$ MPa, with $S_w = 15\%$ and $f = 25$ Hz (Figs. 4 and 7); (ii) $S_w = 0$ and $S_w = 100\%$, with $p = 68$ MPa and $f = 25$ Hz (Fig. 5); and (iii) $f = 25$ Hz and $f = 1$ MHz, with $p = 68$ MPa and $S_w = 15\%$ (Fig. 6). The figures show polar representations of the energy velocities and quality factors for a vertical plane containing the symmetry axis. Only one-quarter of the curves are displayed because of symmetry. The compressional waves are denoted by qP and qP2 and the shear wave by qS. The shear wave, denoted by S, is the pure cross-plane mode.

At high pore pressure (microcracks open) the velocities decrease and the medium shows a higher degree of anisotropy and shear-wave splitting than at low pore pressure. Moreover, attenuation increases for increasing pore pressure (Fig. 4).

Substitution of gas by water implies higher qP-wave velocities and lower shear-wave velocities—the latter behavior is due to the well-known density effect. Moreover, attenuation is lower for full gas saturation than for full water saturation (Fig. 5).

At constant fluid saturation (in particular for $S_w = 15\%$) and high pore pressure (Fig. 6), the velocity dispersion is important when going from the seismic band to the ultrasonic band (approximately 600 m/s for the qP wave and 400 m/s for the shear waves). This in part due to viscoelasticity and in part due to patchy-saturation effects (see Eq. (42)). The slow qP wave has a velocity of hundred of m/s at 1 MHz. Moreover, qS and S attenuation increases more than qP attenuation.

6. Conclusions

We have obtained the phase velocity, attenuation factor, energy velocity and quality factor of an anisotropic porous rock as a function of pore pressure and water saturation. For homogeneous plane waves, they can be explicitly written in terms of the complex velocity, eigenvectors of the Christoffel matrix, stiffness and density matrices, and direction cosines defining the propagation direction. The expressions are easily programmed, and can be used to analyze the acoustic properties of reservoir rocks as a function of confining and pore pressures, saturation and frequency. The theory can be used to predict pore pressure and saturation from seismic data.

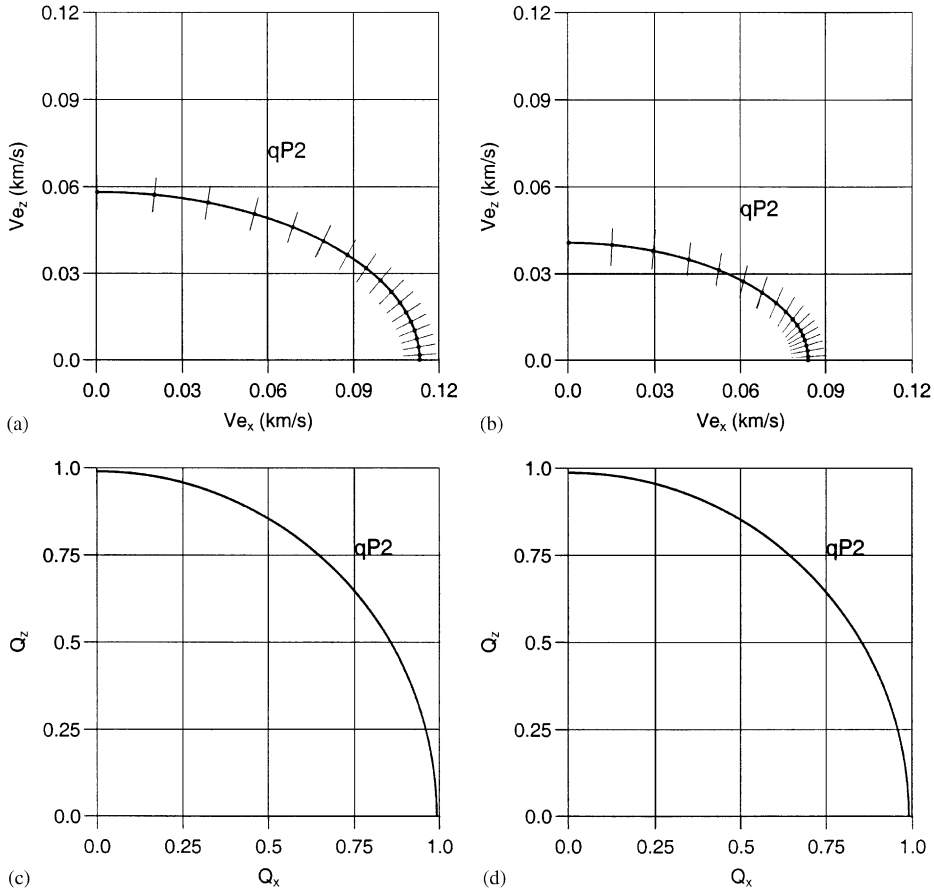

Fig. 7. Polar representations of the wet-rock energy velocities and quality factors of the slow compressional wave for $p = p_H$ (a and c) and $p = 68$ MPa (b and d), with $S_w = 15\%$ and $f = 25$ Hz.

Acknowledgements

We thank Fabio Cavallini for useful comments.

Appendix A. Stiffness components of anisotropic poroelasticity

Cheng [10] gives the stiffness matrix $\mathbf{C}^u$ in terms of properties of the grain, porefluid and skeleton:

c_{IJ}	stiffness components of the drained skeleton.
K_s	bulk modulus of the grain.
K_f	bulk modulus of the porefluid.
ϕ	porosity.

Then, under the assumptions of micro-homogeneity and micro-isotropy, we have

$$c^u_{IJ} = c_{IJ} + M\alpha_I\alpha_J, \tag{A.1}$$

$$M = \frac{K_s}{(1 - \bar{K}/K_s) - \phi(1 - K_s/K_f)}, \tag{A.2}$$

$$\bar{K} = \frac{1}{9}[c_{11} + c_{22} + c_{33} + 2(c_{12} + c_{13} + c_{23})], \tag{A.3}$$

$$\begin{aligned}
\alpha_1 &= 1 - (c_{11} + c_{12} + c_{13})/(3K_s),\\
\alpha_2 &= 1 - (c_{12} + c_{22} + c_{23})/(3K_s),\\
\alpha_3 &= 1 - (c_{13} + c_{23} + c_{33})/(3K_s),\\
\alpha_4 &= -(c_{14} + c_{24} + c_{34})/(3K_s),\\
\alpha_5 &= -(c_{15} + c_{25} + c_{35})/(3K_s),\\
\alpha_6 &= -(c_{16} + c_{26} + c_{36})/(3K_s).
\end{aligned} \tag{A.4}$$

The effective stress coefficients α_I are a property of the solid skeleton only. The fact that these components constitute a 6-D vector implies that pore pressure induces not only dilatational deformations, but also shear deformations. This is not the case in an isotropic medium [10].

References

[1] Winterstein DF. Velocity anisotropy: terminology for geophysicists. Geophysics 1990;55:1070–88.
[2] Carcione JM, Cavallini F. Energy balance and fundamental relations in anisotropic-viscoelastic media. Wave Motion 1993;18:11–20.

[3] Carcione JM, Cavallini F, Helbig K. Anisotropic attenuation and material symmetry. Acustica 1998;84:495–502.
[4] Biot MA. Theory of elasticity and consolidation for a porous anisotropic solid. J Appl Phys 1955;26:182–5.
[5] Biot MA. Theory of deformation of a porous viscoelastic anisotropic solid. J Appl Phys 1956;27:459–67.
[6] Biot MA, Willis DG. The elastic coefficients of the theory of consolidation. J Appl Mech 1957;24:594–601.
[7] Brown R, Korringa J. On the dependence of the elastic properties of a porous rock on the compressibility of the pore fluid. Geophysics 1975;40:608–16.
[8] Carroll MM. Mechanical response of fluid-saturated porous materials. In: Rimrott FPJ, Tabarrok B, editors. Theoretical and applied mechanics. Proceedings of the 15th International Congress on Theoretical and Applied Mechanics, Toronto, 1980. p. 251–62.
[9] Thompson M, Willis JR. A reformulation of the equations of anisotropic poroelasticity. J Appl Mech ASME 1991;58:612–6.
[10] Cheng AH-D. Material coefficients of anisotropic poroelasticity. Int J Rock Mech Min Sci Geomech Abstr 1997;34:199–205.
[11] Lo TW, Coyner KB, Toksöz MN. Experimental determination of elastic anisotropy of Berea sandstone, Chicopea shale, and Chelmsford granite. Geophysics 1986;51:164–71.
[12] Aoki T, Tan CP, Bramford WE. Effects of deformation and strength anisotropy on boreholes failures in saturated rocks. Int J Rock Mech Min Sci Geomech Abstr 1993;30:1031–4.
[13] Rasolofosaon PNJ, Zinszner BE. Comparison between permeability anisotropy and elasticity anisotropy of reservoirs rocks. Geophysics 2002;67:230–40.
[14] Norris AN. Dispersive plane wave propagation in periodically layered anisotropic media. Proc R Ir Acad 1992;92A(1): 49–67.
[15] Ben-Menahem A, Gibson RL. Directional attenuation of *SH*-waves in anisotropic poroelastic media. J Acoust Soc Am 1993;93:3057–65.
[16] Parra JO. The transversely isotropic poroelastic wave equation including the Biot and the squirt mechanisms: theory and application. Geophysics 1997;62:309–18.
[17] Gelinsky S, Shapiro SA. Poroelastic backus-averaging for anisotropic, layered fluid and gas saturated sediments. Geophysics 1997;62:1867–78.
[18] Gelinsky S, Shapiro SA, Müller T, Gurevich B. Dynamic poroelasticity of thinly layered structures. Int J Solids Struct 1998;35:4739–51.
[19] Carcione JM. Energy balance and fundamental relations in dynamic anisotropic poro-viscoelasticity. Proc R Soc London Ser A 2001a; 457:331–48.
[20] Carcione JM. Wave fields in real media: wave propagation in anisotropic, anelastic and porous media, Handbook of Geophysical Exploration, vol. 31. Amsterdam: Pergamon, 2001.
[21] Hudson JA. The effect of fluid pressure on wavespeeds in a cracked solid. Geophys J Int 2000;143:302–10.
[22] Tod SR. The effects of stress and fluid pressure on the anisotropy of interconnected cracks. Geophys J Int 2002;149: 149–56.
[23] Kjartansson E. Constant Q-wave propagation and attenuation. J Geophys Res 1979;84:4737–48.
[24] Carcione JM, Cavallini F, Mainardi F, Hanyga A. Time-domain modeling of constant-Q seismic waves using fractional derivatives. Pure Appl Geophys 2002;159:1719–36.
[25] Keller JD. Acoustic wave propagation in composite fluid-saturated media. Geophysics 1989;54:1554–63.
[26] Johnson DL, Koplik J, Dashen R. Theory of dynamic permeability and tortuosity in fluid-saturated porous media. J Fluid Mech 1987;176:379–402.
[27] Carcione JM, Gangi A. Gas generation and overpressure: effects on seismic attributes. Geophysics 2000;65:1769–79.
[28] Carcione JM, Gangi A. Non-equilibrium compaction and abnormal pore-fluid pressures: effects on seismic attributes. Geophys Prosp 2000;48:521–37.
[29] Luo X, Vasseur G. Geopressuring mechanism of organic matter cracking: numerical modeling. AAPG Bull 1996;80:856–74.
[30] Rubey WW, Hubbert MK. Role of fluid pressure mechanics of overthrust faulting, II. Overthrust belt in geosynclinal area of Western Wyoming in light of fluid pressure hypothesis. Geol Soc Am 1959;70:167–205.
[31] Zimmerman RW. Compressibility of sandstones. Amsterdam: Elsevier, 1991.
[32] Cadoret T, Marion D, Zinszner B. Influence of frequency and fluid distribution on elastic wave velocities in partially saturated limestones. J Geophys Res 1995;100:9789–803.
[33] Dvorkin J, Moos D, Packwood JL, Nur A. Identifying patchy saturation from well logs. Geophysics 1999;64:1756–9.
[34] Brie A, Pampuri F, Marsala AF, Meazza O. Shear sonic interpretation in gas-bearing sands. Proceedings of the SPE Annual Technical Conference, #30595, 1995. p. 701–10.
[35] Auld BA. Acoustic fields and waves in solids. Malabar, FL: Robert E. Krieger, 1991.
[36] Dvorkin J, Nolen-Hoeksema R, Nur A. The squirt-flow mechanism: macroscopic description. Geophysics 1994;59:428–38.
[37] Biot MA. Mechanics of deformation and acoustic propagation in porous media. J Appl Phys 1962;33:1482–98.
[38] Ben-Menahem A, Singh SG. Seismic waves and sources. New York: Springer, 1981.
[39] Prasad M, Manghnani MH. Effects of pore and differential pressure on compressional wave velocity and quality factor in Berea and Michigan sandstones. Geophysics 1997;62:1163–76.
[40] Berryman JG. Effective stress for transport properties of inhomogeneous porous rock. J Geophys Res 1992;97(B12): 17409–24.
[41] Guéguen Y, Palciauskas V. Introduction to the physics of rocks. Princeton, NJ: Princeton University Press, 1994.
[42] Mavko G, Mukerji T, Dvorkin J. The rock physics handbook: tools for seismic analysis in porous media. Cambridge: Cambridge University Press, 1998.
[43] Mavko G, Nur A. Effect of a percolation threshold in the Kozeny–Carman relation. Geophysics 1997;62:1480–2.
[44] Gangi A. The variation of mechanical and transport properties of cracked rock with pressure. In: Einstein HH, editor. Rock mechanics from research to application, Proceedings of the 22nd US Symposium on Rock Mechanics, Cambridge, MA. 1981. p. 88–89.
[45] Stoll RD, Bryan GM. Wave attenuation in saturated sediments. J Acoust Soc Am 1970;47:1440–7.
[46] Auriault JL, Borne L, Chambon R. Dynamics of porous saturated media, checking of the generalized law of Darcy. J Acoust Soc Am 1985;77:1641–50.
[47] Bland DR. The theory of linear viscoelasticity. Oxford: Pergamon Press, 1960.
[48] Scott-Blair GW. Survey of general and applied rheology. London: Pitman, 1949.
[49] Carcione JM, Cavallini F. A rheological model for anelastic anisotropic media with applications to seismic wave propagation. Geophys J Int 1994;119:338–48.
[50] Reid RC, Prausnitz JM, Poling BE. The properties of gases and liquids. New York: McGraw-Hill, 1987.
[51] Carcione JM, Poletto F. Sound velocity of drilling mud saturated with reservoir gas. Geophysics 2000;65:646–51.
[52] Mann DM, Mackenzie AS. Prediction of pore fluid pressures in sedimentary basins. Mar Petrol Geol 1990;7:55–65.

[53] Bear J, Bachmat Y. Introduction to modeling of transport phenomena in porous media. Dordrecht: Kluwer Academic Publishers, 1990.
[54] Bear J, Braester C, Menier PC. Effective and relative permeabilities of anisotropic porous media. Transp Porous Media 1987;2:301–16.
[55] Hudson JA, Liu E. Effective elastic properties of heavily faulted structures. Geophysics 1999;64:479–85.
[56] Jakobsen MH, Hudson JA, Minshull TA, Singh SC. Elastic properties of hydrate-bearing sediments using effective medium theory. J Geophys Res 2000;105:561–77.
[57] Liu E, Hudson JA, Pointer T. Equivalent medium representation of fractured rock. J Geophys Res 2000;105:2981–3000.
[58] Thomson W. (Lord Kelvin), Elements of a mathematical theory of elasticity. Phil Trans R Soc 1856;166:481–98.